

Multivalent Ion Mobility in Layered NbS₂ and NbSe₂ Structures with Trigonal Prismatic Transition Metal Coordination

Daehyun Kim and Haesun Park*



Cite This: ACS Appl. Energy Mater. 2025, 8, 7217–7225



Read Online

ACCESS |

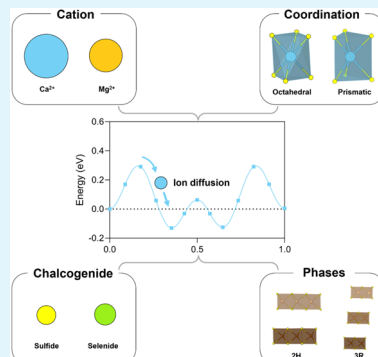
Metrics & More

Article Recommendations

Supporting Information

ABSTRACT: The development of multivalent energy-storage systems is hindered by the scarcity of electrode materials capable of supporting the reversible intercalation of multivalent ions. Layered structures containing trigonal prismatic polyhedra offer a promising framework for efficient ion diffusion, leveraging the favorable coordination environments predicted by Pauling's theory. Thus, this study is aimed at systematically examining the migration mechanisms of divalent ions (Ca and Mg) within NbS₂ and NbSe₂ layered structures, focusing on the influence of structural phases (2H and 3R) and coordination geometries (prismatic and octahedral). The migration behavior is modulated by coordination environments, ionic interactions, and local structural distortions, which collectively determine the energy barriers and diffusion pathways. Results demonstrate that trigonal prismatic coordination significantly reduces migration barriers compared with octahedral coordination, owing to the absence of coordination fluctuations during diffusion. Additionally, the choice of chalcogenide species affects migration barriers, with Se ions generally exhibiting lower migration barriers than those associated with S ions except in specific structural contexts. This work elucidates the intricate interplay among structural phases, coordination geometries, and chalcogenide composition, offering valuable insights into the design of advanced materials for multivalent ion storage.

KEYWORDS: multivalent electrode, cation diffusion, layered transition metal dichalcogenides, trigonal prismatic coordination, density functional theory, migration barrier



1. INTRODUCTION

Transition metal oxides with layered structures have been widely used as electrode materials in Li-based energy-storage devices owing to their high energy density and cycling performance.^{1,2} These properties are attributable to their structural features, which enable facile diffusion of Li within the lattice and topotactic (de)intercalation of Li ions. Although Li-based energy-storage systems with layered transition metal oxides have been applied as commercial rechargeable batteries, the limited availability of lithium poses challenges in meeting the growing demand for energy-storage systems.³

Multivalent ions, such as Mg and Ca, present a viable alternative⁴ owing to their abundance in the Earth's crust (Ca: 4.2%, Mg: 2.3%, Li: 0.002%), thereby ensuring adequate supply and reduced manufacturing costs. Moreover, Mg and Ca possess relatively low standard electrode potentials (Mg: -2.37 V, Ca: -2.87 V vs SHE), which enable high-voltage battery operation. In contrast, other multivalent counterparts such as Zn²⁺ (-0.76 V) and Al³⁺ (-1.66 V) exhibit significantly higher potentials, limiting the achievable cell voltage and thus reducing their suitability for high-energy applications. However, the development of multivalent ion batteries is hindered by the lack of host materials allowing reversible intercalation of multivalent guest ions.⁵ The multivalent nature of the cations leads to strong electrostatic

interactions with the host framework, resulting in sluggish ion diffusion—a phenomenon that is particularly pronounced in trivalent Al³⁺-based systems.^{6,7} Although materials such as polyanionic compounds^{8,9} and Prussian blue analogs¹⁰ have been shown to support topotactic (de)intercalation of Ca ions, layered structures are particularly promising for fully leveraging the high energy density of Ca-based systems.^{11–14} A significant bottleneck in enabling the (de)intercalation of multivalent ions lies in overcoming the high energy barriers to cation diffusion, which are influenced by the coordination environment of the cations within the layered structure.

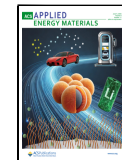
According to Pauling's rule, Ca ions favor coordination numbers greater than six, typically adopting either octahedral (O-type) or prismatic (P-type) coordination in layered structures with a nominal stoichiometry of TMO₂. Notably, in O-type structures, long-range diffusion of Ca occurs via migration through tetrahedral sites, which induces a substantial energy penalty and high activation energy.¹⁵ Conversely, in P-

Received: February 24, 2025

Revised: May 5, 2025

Accepted: May 6, 2025

Published: May 19, 2025



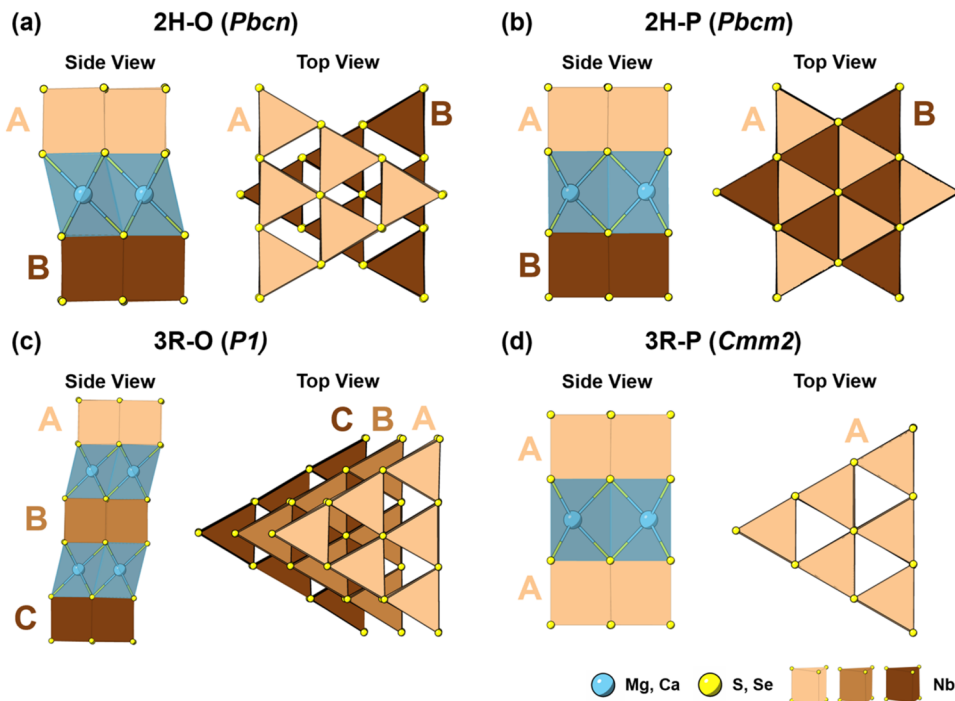


Figure 1. Crystal structures of layered transition metal dichalcogenides in 2H and 3R phases: (left) side view of stacking layers in a fully occupied state; (right) top view of stacking layers in a vacant state. (a) Cations with octahedral coordination in the 2H structure. (b) Cations with trigonal prismatic coordination in the 2H structure. (c) Cations with octahedral coordination in the 3R structure. (d) Cations with trigonal prismatic coordination in the 3R structure. “-O” and “-P” refer to cations in octahedral coordination and trigonal prismatic coordination between transition metal layers, respectively. Blue and brown polyhedra represent intercalated multivalent ions (Mg and Ca) and Nb, respectively. Yellow spheres represent chalcogenide atoms (S and Se). Space groups for each structure are indicated at the top.

type structures, Ca diffusion proceeds through a transition state that retains prismatic coordination in both the initial and final states, resulting in a smoother energy landscape and lower migration barrier.¹⁵ Nonetheless, phase transitions between O-type and P-type layered structures, which may occur under varying degrees of intercalation, can impede Ca diffusion.

In the context of P-type and O-type structures, various studies have focused on the diffusion pathways in layered structures with octahedral coordination within transition metal layers, examining migration barrier energies across a range of transition metal materials.^{15–22} However, research on ion mobility in layered structures with trigonal prismatic transition metal layers serving as intercalation hosts for multivalent ions remains limited. While ion diffusion in layered oxides with octahedral transition metal coordination has been widely studied, much less is known about layered chalcogenides, particularly those featuring trigonal prismatic coordination.^{15,18,23} Moreover, direct comparisons of diffusion mechanisms between prismatic and octahedral geometries within the same host composition are rare. Investigating ion migration in layered structures with trigonal prismatic transition metal layers offers a valuable opportunity to elucidate how diffusion mechanisms differ from those in conventional octahedral frameworks, especially in the context of multivalent ion transport.

As dictated by Ramsdell’s notation, transition metal dichalcogenides (TMDs) with trigonal prismatic transition metal layers are categorized into 2H and 3R phases. The 2H phase exhibits an ABAB stacking sequence within a hexagonal unit cell, whereas the 3R phase is characterized by an ABCA stacking sequence within a rhombohedral unit cell.²⁴ Trigonal prismatic coordination involves one transition metal sur-

rounded by six anion species, with its formation largely influenced by the choice of transition metal and its d-covalency.^{25,26} Notably, TMDs with trigonal prismatic coordination have demonstrated stable cycling performance and favorable electrochemical potentials in (de)intercalation reactions.^{27–31} These properties make them particularly promising for the development of electrodes using multivalent ions such as Mg and Ca, given their success in applications such as Na-ion batteries.

To better understand the migration behavior of multivalent ions within layered structures with trigonal prismatic coordination, the interplay between coordination environments, migration pathways, and structural phases must be explored. Although Ca and Mg ions share similar divalent characteristics, their migration behaviors differ significantly, owing to variations in ionic size and interactions with the host framework. These differences are particularly pronounced in layered structures like NbS₂ and NbSe₂, which exhibit distinct coordination environments (e.g., trigonal prismatic and octahedral) and variable migration energy barriers. Notably, Nb-based transition metal dichalcogenides have been previously studied as intercalation host frameworks for Li and Na ions,^{32,33} while maintaining the trigonal prismatic coordination of the alkali-ion layers. This compatibility with alkali-ion intercalation suggests their potential as frameworks for multivalent ion diffusion. In particular, many multivalent ion systems, especially for Ca, have adopted Na-ion intercalation hosts as templates owing to the comparable ionic radii and coordination characteristics. For example, NASICON-type structures have been extensively adapted for Ca-ion storage.^{8,9,34} In this context, NbS₂ and NbSe₂ are attractive candidates as they support Na intercalation and offer structural

pathways that allow guest ions to migrate while retaining prismatic coordination, making them well suited for multivalent ion transport.

Considering these aspects, in this study, the migration barriers and mechanisms of Ca and Mg ions were examined, focusing on their diffusion pathways in NbS_2 and NbSe_2 layered structures with trigonal prismatic coordination. The influence of structural phases (2H and 3R), coordination geometries of cations (prismatic and octahedral), and chalcogenide species (S and Se) on ion diffusion and associated energy barriers was investigated. Our findings reveal that trigonal prismatic coordination generally results in lower migration barriers compared with octahedral coordination, as it minimizes coordination fluctuations during diffusion. However, notable differences are observed in the migration behaviors of Ca and Mg ions, with Mg ions exhibiting lower barriers in most pathways except in cases characterized by strong Coulombic interactions. Furthermore, the choice of chalcogenide species introduces further variability in migration energy, with Se ions typically showing lower barriers than S ions, although exceptions are identified in certain structural environments.

By highlighting the intricate relationships among ionic coordination, structural phases, and chalcogenide composition, this work provides critical insights for designing advanced host materials for multivalent ion storage. The findings can offer guidance for developing energy-storage systems characterized by higher energy densities and improved mobility of multivalent ions, thereby addressing the growing demand for sustainable and efficient energy-storage technologies.

2. EXPERIMENTAL SECTION

First-principles calculations were performed using density functional theory, as implemented in the Vienna Ab initio Simulation Package (VASP).^{35,36} The electron exchange-correlation functional was described using the generalized gradient approximation (GGA) of the Perdew–Burke–Ernzerhof (PBE) functional.³⁷ The core electron contribution was modeled using the projector-augmented wave (PAW) potential, whereas the valence electrons were represented by a plane-wave basis set with a cutoff energy of 520 eV.³⁸ The convergence criterion for ionic relaxation was set as 10^{-5} eV for electronic calculation, and the Hellmann–Feynman force on each atom was below 0.02 eV Å⁻¹. A spin polarization calculation was used. van der Waals interactions were assumed to be negligible due to the strong electrostatic and covalent interactions between cations and surrounding anions.³⁹

We adopted unit cells from the polymorphs of CaNb_2S_4 (*Pbcn*: $\text{Ca}_4\text{Nb}_8\text{S}_{16}$ for 2H-O, *Pbcm*: $\text{Ca}_4\text{Nb}_8\text{S}_{16}$ for 2H-P, *P1*: $\text{Ca}_4\text{Nb}_8\text{S}_{16}$ for 3R-O, *Cmm2*: $\text{Ca}_2\text{Nb}_4\text{S}_8$ for 3R-P). Each structure was taken from the Materials Project database.⁴⁰ The weak van der Waals interactions enabled sliding between layers, resulting in a model structure with cations exhibiting either octahedral or trigonal prismatic coordination.^{41,42} In the 2H layered structure, shown in Figure 1a,b, transition metal layers are stacked in alternating opposite orientations. The space groups of cations with octahedral and trigonal prismatic coordination in the 2H layered structures are *Pncn* and *Pbcm*, respectively. In contrast, in the 3R layered structures, transition metal layers are oriented in the same direction, as illustrated in Figure 1c,d. Cations with octahedral and trigonal prismatic coordination in these structures belong to *P1* and *Cmm2* space groups, respectively. Notations “-O” and “-P” refer to cations exhibiting octahedral coordination and trigonal prismatic coordination between transition metal layers, respectively.

Migration barriers were calculated using the nudged elastic band (NEB) method.⁴³ The climbing-image NEB method did not significantly affect the migration barrier (Figure S1), and the

conventional NEB method was used throughout for computational efficiency.⁴⁴ We considered the minimum energy paths for single-ion migration in the 2H-O, 2H-P, 3R-O, and 3R-P structures. In 2H-P and 3R-P structures, stable trigonal prismatic sites were used as waypoints, and for each segment between these states, three intermediate images were inserted, resulting in a total of 13 images including the initial and final states. For the 2H-O and 3R-O structures, the diffusion step was considered between the initial and final octahedral sites using five intermediate images, resulting in a total of 7 images. To prevent interactions between periodic images from influencing the migration barrier, the NEB calculations involved supercells with dimensions of $2 \times 2 \times 1$ for the 2H-O, 2H-P, and 3R-O structures and $2 \times 2 \times 2$ for the 3R-P structure. All NEB calculations were relaxed to an atomic force tolerance of 0.05 eV Å⁻¹.

3. RESULTS AND DISCUSSION

3.1. Diffusion Path of Cations with Trigonal Prismatic Coordination. The thermodynamic stability of each composition was assessed by calculating the energy above the convex hull (E^{hull}), which measures the energetic distance from the most stable decomposition compounds. An E^{hull} of zero indicates a stable compound, while a positive value suggests a tendency to decompose into more stable phases. However, compounds with E^{hull} values below ~ 50 meV/atom are often considered metastable but synthesizable, particularly when entropic and kinetic factors are taken into account.⁴⁵

As summarized in Table 1, all calculated structures fall within this metastable window. Ca-intercalated structures

Table 1. Energy above the Convex Hull (in meV/atom) for CaNb_2S_4 , CaNb_2Se_4 , MgNb_2S_4 , and MgNb_2Se_4

	2H-O (meV/atom)	2H-P (meV/atom)	3R-O (meV/atom)	3R-P (meV/atom)
CaNb_2S_4	12	0	17	2
CaNb_2Se_4	7	6	16	8
MgNb_2S_4	0	36	8	40
MgNb_2Se_4	14	51	19	59

^aThe values are compared across different stacking sequences (2H and 3R) and cation coordination (octahedral and trigonal prismatic), denoted as 2H-O, 2H-P, 3R-O, and 3R-P, respectively.

exhibit particularly low E^{hull} values, especially in prismatic environments (0–8 meV/atom), indicating their favorable thermodynamic behavior. In contrast, Mg-intercalated structures exhibit a preference for octahedral coordination, as evidenced by the thermodynamic stability of MgNb_2S_4 in the 2H-O phase ($E^{\text{hull}} = 0$ meV/atom). Meanwhile, Mg-based prismatic structures exhibit higher E^{hull} values (51 and 59 meV/atom), suggesting relatively lower stability under such coordination. These results highlight the structural preferences of Ca and Mg intercalants, which are governed by their ionic sizes and preferred coordination environments.

To assess their efficiency as electrode materials, we calculated the average intercalation voltage and gravimetric capacity for the thermodynamically favorable compositions in the 2H-O structure. MgNb_2S_4 exhibited an average voltage of 1.23 V with 158 mAh g⁻¹, while MgNb_2Se_4 showed 0.82 V and 102 mAh g⁻¹. For Ca-based compounds, CaNb_2S_4 delivered 1.99 V and 151 mAh g⁻¹, whereas CaNb_2Se_4 showed 1.62 V and 99 mAh g⁻¹. These values are comparable to those of conventional intercalation materials such as $\text{Li}_4\text{Ti}_5\text{O}_{12}$ (LTO), which typically exhibit ~ 1.55 V and ~ 175 mAh g⁻¹. These results highlight the strong potential for further exploration as an alternative electrode material.

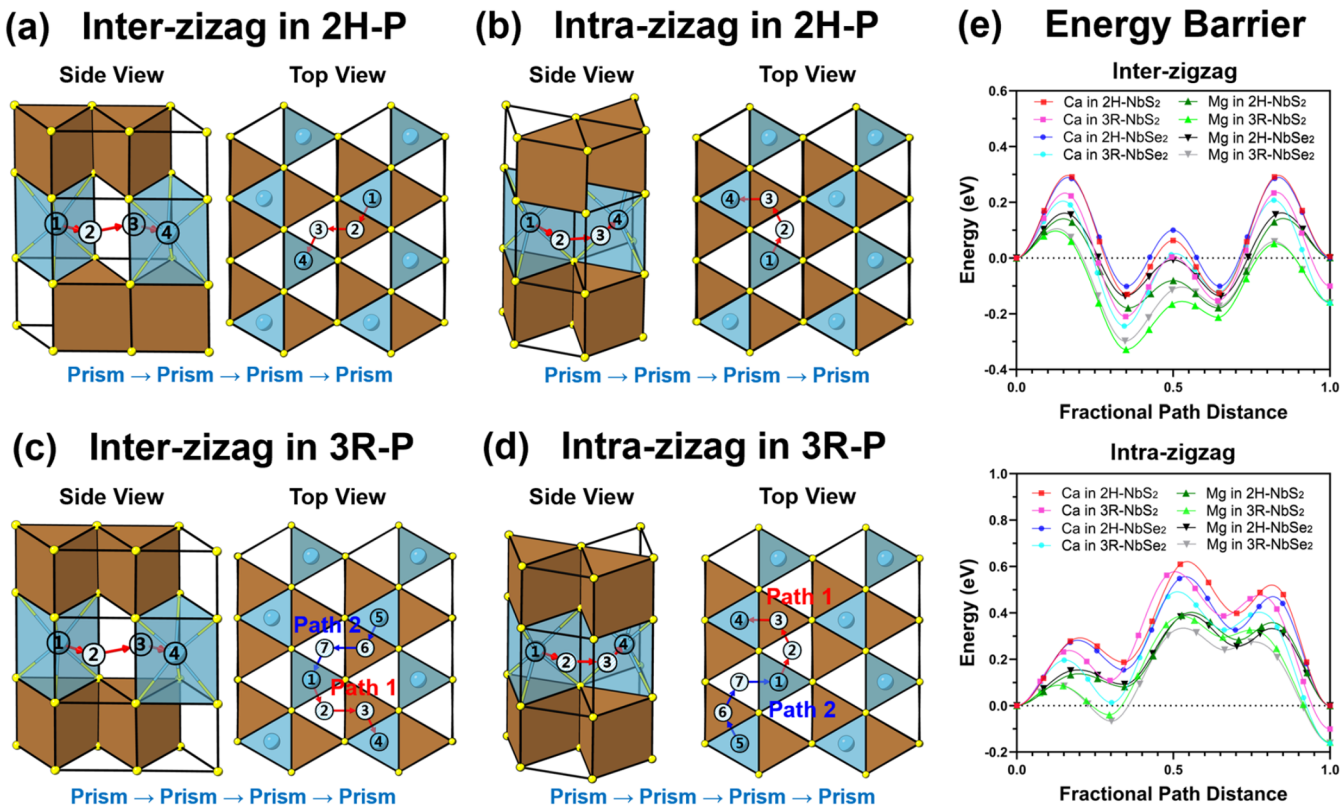


Figure 2. Diffusion mechanisms of inter- and intra-zigzag pathways in 2H-P and 3R-P: (a) inter-zigzag in 2H-P, (b) intra-zigzag in 2H-P, (c) inter-zigzag in 3R-P, and (d) intra-zigzag in 3R-P. In the 3R-P structure, two pathways, Path 1 (red line) and Path 2 (blue line), are present. Numbers on ions indicate the diffusion path: (left) side view, (right) top view. (e) Migration barriers for inter-zigzag and intra-zigzag pathways for all configurations, with Path 2 indicated as the migration barrier for the 3R-P structure (ions: Ca, Mg; chalcogenides: S, Se; structures: 2H-P, 3R-P). In 2H-P, each migration step occurs through a clear coordination environment, whereas in 3R-P, the local environment alternates due to face-sharing with either Nb polyhedra or vacancies. Brown polyhedra represent Nb, and blue and yellow spheres represent migration ions and chalcogenide atoms, respectively. Owing to their divalent nature, Ca and Mg ions insert at 0.5 atoms per NbS_2 or NbSe_2 structure and partially occupy ionic layers even in a fully filled state, forming a zigzag-like arrangement, as depicted in the top view of (a–d). This arrangement results in a distinct migration mechanism characterized by two modes: inter-zigzag hopping (ions migrating across neighboring zigzag lines) and intra-zigzag hopping (ions migrating along the same zigzag line).

First, we examine the minimum energy pathways of cations with trigonal prismatic coordination. Figure 2a,b illustrates the inter- and intra-zigzag migration of multivalent ions in the 2H-P structure, where the cations retain trigonal prismatic coordination throughout the diffusion process. In this structure, the migration environment is influenced by the surrounding transition metal layers. The cation alternately shares one face with the top or bottom face of the prismatic polyhedron of Nb, resulting in identical coordination environments across all states. Conversely, as illustrated in Figure 2c,d, the inter- and intra-zigzag migration modes in the 3R-P structure result in distinct environments within the transition metal layers. These differences arise from variations in whether the migrating ion shares a face with the Nb polyhedron. In the initial state, the ion shares both the top and bottom faces with the Nb polyhedron, whereas in the final state, it does not share any face.

In addition, in the 3R-P structure, the distinct environments between the initial and final states lead to two migration pathways, as shown in Figure 2c,d: Path 1 (red line) and Path 2 (blue line). Path 1 describes ion migration from the initial state, where the ion shares both top and bottom faces, to the final state, where it shares no face. In contrast, Path 2 represents reverse migration. As shown in Figure 2c, during inter-zigzag migration in 3R-P, Path 2 ($\textcircled{5} \rightarrow \textcircled{6} \rightarrow \textcircled{7} \rightarrow \textcircled{1}$) and

Path 1 ($\textcircled{1} \rightarrow \textcircled{2} \rightarrow \textcircled{3} \rightarrow \textcircled{4}$) proceed in opposite directions, resulting in equivalent migration energy barriers (Table 1). However, for intra-zigzag migration, a notable difference in migration energy is observed between Paths 1 and 2. Both paths favor routes with fewer edge-sharing cations. For example, in state $\textcircled{2}$, the cation shares an edge with one neighboring cation polyhedron, whereas in state $\textcircled{3}$, it shares edges with two neighboring cations. As shown in Table 2, for Ca ions, the migration energy difference between Paths 1 and 2 is 0.03 eV in NbS_2 and 0.04 eV in NbSe_2 . In contrast, for Mg ions, the migration energy difference is larger, with values of 0.07 eV for NbS_2 and 0.08 eV for NbSe_2 .

Table 2. Migration Energy Barriers for Inter- and Intra-Zigzag Hopping along Paths 1 and 2 in CaNb_2S_4 , CaNb_2Se_4 , MgNb_2S_4 , and MgNb_2Se_4 in a 3R-P Structure

	inter-zigzag (eV)		intra-zigzag (eV)	
	Path 1	Path 2	Path 1	Path 2
CaNb_2S_4	0.45	0.45	0.65	0.68
CaNb_2Se_4	0.45	0.45	0.61	0.65
MgNb_2S_4	0.43	0.43	0.47	0.54
MgNb_2Se_4	0.40	0.40	0.42	0.50

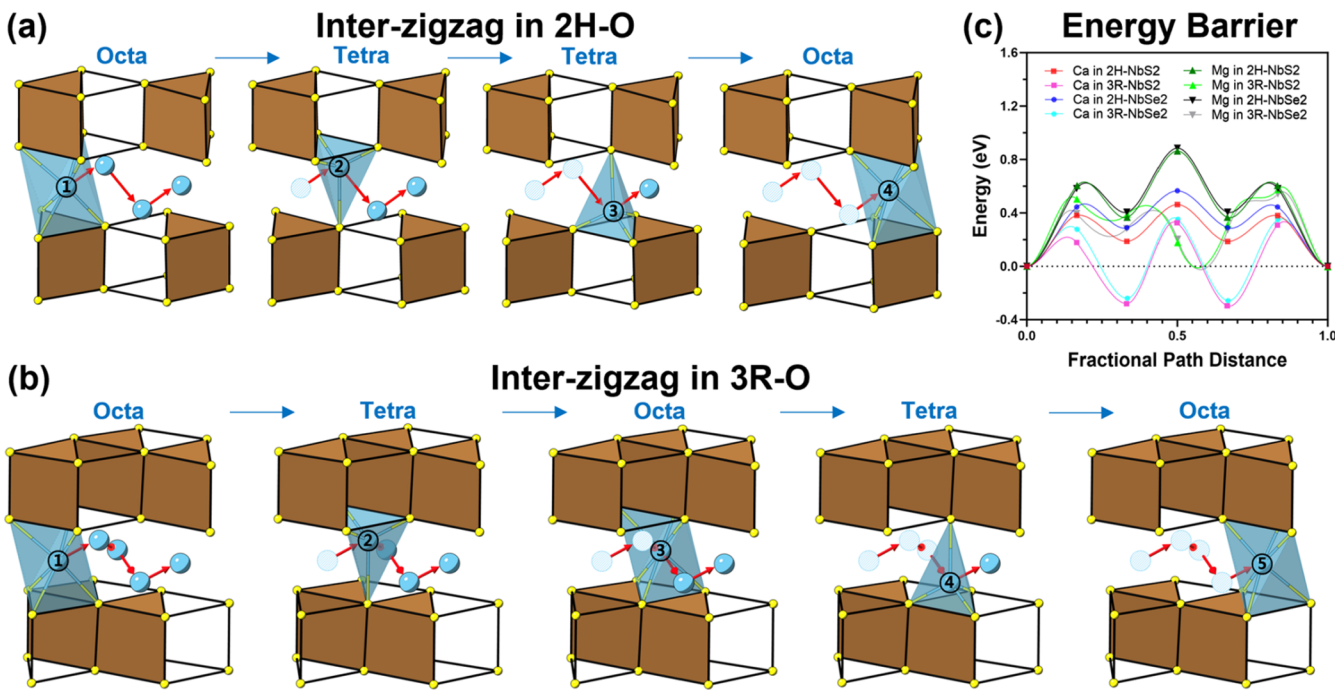


Figure 3. Inter-zigzag migration mechanisms of cations with octahedral coordination in (a) 2H-O and (b) 3R-O. (c) Migration energy barriers for inter-zigzag pathways across all configurations (ions: Ca, Mg; chalcogenides: S, Se; structures: 2H-O, 3R-O). In 2H-O, ions migrate directly between tetrahedral sites, while in 3R-O, they pass through octahedral sites due to Coulombic repulsion from adjacent Nb polyhedra. Brown polyhedrons represent Nb, and blue and yellow spheres represent migration ions and chalcogenide atoms, respectively. Numbers on the ions indicate the diffusion path.

To comprehensively understand the origin of the energy difference between Paths 1 and 2 during intra-zigzag migration in the 3R-P structure, we analyzed the local environments of the migration process. As illustrated in Figure 2e, in the minimum energy paths for Path 2, the final state consistently exhibits energy lower than that of the initial state across all calculations. These results suggest that the environment in which an ion shares both the top and bottom faces with the Nb polyhedron (final state) is energetically more stable than when the ion shares its top and bottom faces with vacancies (initial state). Moreover, the ions situated between vacancies are inherently less stable.

As shown in Figure 2d, the migrating ion in state ⑦ shares edges with two neighboring ions in the ionic layer, while its top and bottom faces are vacant. In contrast, the ion in state ③ shares its top and bottom faces with the Nb polyhedron and also shares edges with the two neighboring ions in the ionic layer. The instability of state ⑦ compared with state ③ explains why Path 2 exhibits a higher migration energy barrier during intra-zigzag migration in the 3R-P structure.

The inter-zigzag hopping mechanism consistently exhibits a lower migration barrier compared with the intra-zigzag mechanism, irrespective of structural and compositional variations. In particular, along the inter-zigzag pathway, the migrating ion shares only one edge with the adjacent multivalent ions in the ionic layer. In contrast, the intra-zigzag pathway involves edge-sharing with two neighboring ions. This distinction in local environments contributes to the lower migration barrier observed in inter-zigzag hopping. Among the calculated migration barriers, both Mg and Ca ions exhibit the lowest values in the inter-zigzag pathway within the 2H-NbSe₂ structure (CaNb₂Se₄: 0.39 eV, MgNb₂Se₄: 0.30 eV in 2H-P). Conversely, the highest barriers are observed in the intra-zigzag

pathway within the 3R-NbS₂ structure (CaNb₂S₄: 0.65 eV, MgNb₂S₄: 0.47 eV in 3R-P), as shown in Figure 2e.

Although both Mg and Ca ions maintain trigonal prismatic coordination throughout the diffusion process in both 2H-P and 3R-P structures, Mg consistently exhibits lower migration barriers. This trend is primarily attributed to its smaller ionic radius, which facilitates smoother ion transport along the pathway. Additionally, both ions demonstrate lower migration barriers in the 2H-P phase relative to the 3R-P phase due to differences in the symmetry of the coordination environment. In the 2H-P structure, the cation alternately shares one face with either the upper or lower Nb polyhedron and the other with a vacancy, resulting in a more uniform coordination environment. In contrast, in the 3R-P structure, the cation alternates between configurations where both faces are shared with Nb polyhedra and those in which both faces are shared with vacancies, leading to fluctuations in the coordination environment and higher energy barriers. To aid in detailed understanding, a bar plot comparing the site energy differences with the activation barriers along the diffusion path is provided (Supporting Information S2–S5).

3.2. Diffusion Path of Cations with Octahedral Coordination. The diffusion of cations with octahedral coordination follows distinct pathways compared to those of cations with trigonal prismatic coordination, as illustrated in Figure 3. Unlike cations with trigonal prismatic coordination, cations with octahedral coordination experience fluctuations in coordination along the diffusion pathway, alternating between octahedral and tetragonal configurations. This alternation arises from the inherent structural characteristics of hexagonal close-packed (hcp) anion stacking.

The migration barriers in 2H-O and 3R-O structures are higher than those in 2H-P and 3R-P structures, primarily due

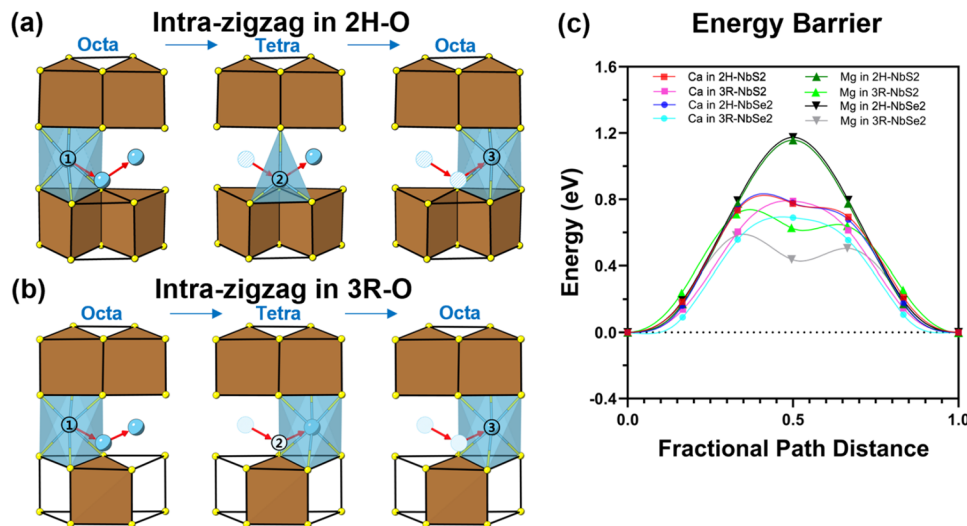


Figure 4. Intra-zigzag migration mechanism of cations with octahedral coordination in (a) 2H-O and (b) 3R-O. (c) Migration energy barriers for intra-zigzag pathways across structures and configurations (ions: Ca, Mg, chalcogenides: S, Se). Brown polyhedrons represent Nb, and blue and yellow spheres represent migration ions and chalcogenide atoms, respectively. Numbers on ions indicate the diffusion path.

to fluctuations in coordination. According to Pauling's radius ratio rule, Mg^{2+} favors octahedral coordination and becomes energetically destabilized when occupying lower-coordination environments such as tetragonal sites. Ca^{2+} , with its larger ionic radius and preference for even higher coordination numbers, also incurs an energetic penalty when constrained to such undercoordinated configurations. In the inter-zigzag hopping mechanism of the 2H-O structure, multivalent ions occupy tetragonal sites during migration, as depicted in Figure 3a (Octa \rightarrow Tetra \rightarrow Tetra \rightarrow Octa). Similarly, in the 3R-O structure, the migrating ion undergoes coordination changes, as shown in Figure 3b (Octa \rightarrow Tetra \rightarrow Octa \rightarrow Tetra \rightarrow Octa).

In the 2H-O structure, cations with tetragonal coordination in states ② and ③ share vacancies, whereas in the 3R-O structure, the cation in state ④ shares a face with a Nb polyhedron. This proximity to the Nb polyhedron, i.e., the smaller distance between the cation and Nb, causes the cation to revert to octahedral coordination. Consequently, cations in the 3R-O structure primarily migrate through alternating coordination changes, leading to an unstable mechanism and deviations during diffusion.

The migration barriers of Ca and Mg ions in the 2H-O and 3R-O structures are compared by considering the effect of coordination changes. Mg ions exhibit higher migration barriers, owing to their stronger binding energy in tetragonal coordination. This results in greater variations in the energy profile along the diffusion pathway.^{7,23,46} Regardless of the migration path or chalcogenide species, Ca ions exhibit lower migration barriers compared with Mg ions, as illustrated in Figure 3c (Ca: 0.46 and 0.57 eV; Mg: 0.86 and 0.89 eV in Nb_2S_4 and Nb_2Se_4 , respectively). However, in the 3R-O structure, the migration barriers for multivalent ions display the opposite trend. In state ④, where cations with tetragonal coordination share a face with the Nb polyhedron, strong Coulombic repulsion hinders Ca migration and increases the corresponding migration barriers (Ca: 0.63 and 0.62 eV; Mg: 0.61 and 0.58 eV in Nb_2S_4 and Nb_2Se_4 , respectively). Consequently, in the 2H-O structure, Ca ions consistently exhibit lower migration barriers than Mg ions, primarily due to

the stronger binding affinity of Mg in the intermediate tetragonal states, which increases the energy penalty during coordination fluctuations. In contrast, although coordination fluctuations also occur in the 3R-O structure, the intermediate tetragonal site shares a face with an adjacent Nb polyhedron, causing stronger Coulombic repulsion for the larger Ca ion. As a result, diffusion of Ca is hindered in 3R-O, whereas the smaller Mg ion experiences less repulsion and thus exhibits more favorable migration behavior in this structure.

The results also indicate that Se ions generally exhibit lower migration barriers compared to S ions. This smoother energy landscape can be attributed to the larger ionic radius of Se, which expands interatomic distances and broadens diffusion pathways, and its higher polarizability, which reduces electrostatic repulsion along the ion migration path and facilitates ion transport.^{47–49} However, in the 2H-O structure, an opposite trend is observed depending on the chalcogenide. In this structure, ions diffuse directly between tetrahedral coordination sites. This mechanism requires ion diffusion across an edge-sharing arrangement between two tetragonal sites. For Se ions, the edge-sharing distance between two anions is distorted and increased compared to that of S ions, attributable to the weaker interactions of Se. Specifically, along the migration path, the average distance between adjacent chalcogen atoms increases more significantly in Se-based structures (0.65 Å for Se vs 0.52 Å for S), resulting in greater geometric distortion. Consequently, Se ions exhibit higher migration energy barriers in comparison to those of S ions.

Similar to cations with trigonal coordination, the intra-zigzag hopping mechanism in the 2H-O and 3R-O structures exhibits a higher energy barrier than that of inter-zigzag hopping. In the intra-zigzag mechanism, cations in octahedral coordination undergo fluctuations in coordination during diffusion, resulting in high migration barriers, as illustrated in Figure 4 (Octa \rightarrow Tetra \rightarrow Octa). In the 2H-O structure, migrating Ca ions demonstrate lower migration barriers than Mg ions (Ca: 0.82 and 0.83 eV; Mg: 1.16 and 1.17 eV in Nb_2S_4 and Nb_2Se_4 , respectively). Conversely, in the 3R-O structure, Mg ions exhibit lower migration barriers owing to their interaction with the Nb polyhedron at state ②, where they share a face with the

Nb polyhedron (Ca: 0.79 and 0.73 eV; Mg: 0.74 and 0.62 eV in Nb_2S_4 and Nb_2Se_4 , respectively).

4. CONCLUSIONS

We systematically analyzed the migration mechanisms of Ca and Mg ions in layered NbS_2 and NbSe_2 structures with trigonal prismatic (2H-P, 3R-P) and octahedral (2H-O, 3R-O) coordination. Our findings highlight that migration behavior and energy barriers are significantly influenced by the coordination environment, structural phase, and chalcogenide species.

For trigonal prismatic coordination, inter-zigzag hopping consistently exhibits lower migration barriers compared with intra-zigzag hopping, attributable to the reduced edge-sharing interactions along the migration pathway. In the 2H-P structure, the uniform coordination environment is maintained throughout the migration process, resulting in equivalent migration energy barriers for Paths 1 and 2 in inter-zigzag hopping. Conversely, in the 3R-P structure, distinct environments between initial and final states lead to differing migration energy profiles, with intra-zigzag pathways demonstrating higher energy barriers owing to the instability of the intermediate states.

For octahedral coordination, cations undergo fluctuations between octahedral and tetragonal configurations during migration, resulting in higher migration barriers in both inter-zigzag and intra-zigzag pathways compared with trigonal prismatic coordination. In 2H-O structures, the intermediate tetragonal states share faces with vacancies, whereas in 3R-O structures, these tetragonal sites share faces with neighboring Nb polyhedra, introducing stronger Coulombic repulsion that further impacts ion mobility.

Notably, this study reveals distinct diffusion characteristics between the Ca and Mg ions. In trigonal prismatic coordination, Mg ions generally exhibit lower migration barriers, owing to their smaller ionic radius. Conversely, in octahedral coordination, Ca ions tend to diffuse more readily due to their preference for higher coordination numbers and lower binding energies in tetrahedral sites. An exception is found in the 3R-O structure, where Coulombic repulsion near the Nb polyhedral destabilizes Ca-ion transport, due to its larger ionic radius. These differences underscore the critical roles of ionic size and coordination stability in multivalent ion transport.

Furthermore, the chalcogenide species significantly influence the migration behavior. While Se ions generally exhibit lower migration barriers than S ions, the opposite trend is observed in the 2H-O structure owing to the increased edge-sharing distance and weaker Se interactions. These outcomes highlight the key influence of local structural distortions on the migration energy barriers.

Our results demonstrate that strategic control of structural features, such as coordination environment, stacking sequence, and chalcogenide composition, can effectively enhance ion mobility without additional engineering. Nevertheless, these findings are limited to Nb-based systems. Future studies should explore a broader range of transition metals and be complemented by experimental validation. By elucidating the role of structural topology in ion transport, this work contributes to the fundamental understanding necessary to accelerate the discovery of versatile host frameworks for reversible multivalent ion storage.

■ ASSOCIATED CONTENT

SI Supporting Information

The Supporting Information is available free of charge at <https://pubs.acs.org/doi/10.1021/acsaem.Sc00560>.

Comparison of Ca migration barriers obtained by conventional NEB and CI-NEB methods; site and migration energy comparison along the diffusion paths for inter- and intra-zigzag migration in 2H-P, 3R-P, 2H-O, and 3R-O phases of CaNb_2S_4 ; site and migration energy comparison along the diffusion paths for inter- and intra-zigzag migration in 2H-P, 3R-P, 2H-O, and 3R-O phases of MgNb_2S_4 ; site and migration energy comparison along the diffusion paths for inter- and intra-zigzag migration in 2H-P, 3R-P, 2H-O, and 3R-O phases of CaNb_2Se_4 ; and site and migration energy comparison along the diffusion paths for inter- and intra-zigzag migration in 2H-P, 3R-P, 2H-O, and 3R-O phases of MgNb_2Se_4 ([PDF](#))

■ AUTHOR INFORMATION

Corresponding Author

Haesun Park – School of Integrative Engineering, Chung-Ang University, Seoul 06974, Republic of Korea;  [orcid.org/0000-0001-6266-8151](#); Email: parkh@cau.ac.kr

Author

Daehyun Kim – School of Integrative Engineering, Chung-Ang University, Seoul 06974, Republic of Korea;  [orcid.org/0009-0007-4596-8030](#)

Complete contact information is available at: <https://pubs.acs.org/10.1021/acsaem.Sc00560>

Notes

The authors declare no competing financial interest.

■ ACKNOWLEDGMENTS

This research was supported by the Chung-Ang University Research Scholarship Grants in 2023, the National Research Foundation of Korea (NRF) grant funded by the Korea Government (MSIT) (RS-2024-00413272), and the National Research Council of Science & Technology (NST) grant by the Korea Government (MSIT) (No. GTL24011-000).

■ REFERENCES

- (1) Mizushima, K.; Jones, P.; Wiseman, P.; Goodenough, J. B. Li_xCoO_2 ($0 < x \leq 1$): A new cathode material for batteries of high energy density. *Mater. Res. Bull.* **1980**, *15* (6), 783–789.
- (2) Li, W.; Erickson, E. M.; Manthiram, A. High-nickel layered oxide cathodes for lithium-based automotive batteries. *Nat. Energy* **2020**, *5* (1), 26–34.
- (3) Liang, Y.; Dong, H.; Aurbach, D.; Yao, Y. Current status and future directions of multivalent metal-ion batteries. *Nat. Energy* **2020**, *5* (9), 646–656.
- (4) Canepa, P.; Sai Gautam, G.; Hannah, D. C.; Malik, R.; Liu, M.; Gallagher, K. G.; Persson, K. A.; Ceder, G. Odyssey of Multivalent Cathode Materials: Open Questions and Future Challenges. *Chem. Rev.* **2017**, *117* (5), 4287–4341.
- (5) Maroni, F.; Dongmo, S.; Gauckler, C.; Marinaro, M.; Wohlfahrt-Mehrens, M. Through the maze of multivalent-ion batteries: a critical review on the status of the research on cathode materials for Mg^{2+} and Ca^{2+} ions insertion. *Batteries Supercaps* **2021**, *4* (8), 1221–1251.
- (6) Arroyo-de Dompablo, M. E.; Porrouch, A.; Johansson, P.; Palacín, M. R. Achievements, challenges, and prospects of calcium batteries. *Chem. Rev.* **2020**, *120* (14), 6331–6357.

- (7) Liu, M.; Rong, Z.; Malik, R.; Canepa, P.; Jain, A.; Ceder, G.; Persson, K. A. Spinel compounds as multivalent battery cathodes: a systematic evaluation based on ab initio calculations. *Energy Environ. Sci.* **2015**, *8* (3), 964–974.
- (8) Kim, S.; Yin, L.; Lee, M. H.; Parajuli, P.; Blanc, L.; Fister, T. T.; Park, H.; Kwon, B. J.; Ingram, B. J.; Zapol, P.; et al. High-voltage phosphate cathodes for rechargeable Ca-ion batteries. *ACS Energy Lett.* **2020**, *5* (10), 3203–3211.
- (9) Jeon, B.; Heo, J. W.; Hyoung, J.; Kwak, H. H.; Lee, D. M.; Hong, S.-T. Reversible calcium-ion insertion in NaSICON-type $\text{NaV}_2(\text{PO}_4)_3$. *Chem. Mater.* **2020**, *32* (20), 8772–8780.
- (10) Lipson, A. L.; Pan, B.; Lapidus, S. H.; Liao, C.; Vaughey, J. T.; Ingram, B. J. Rechargeable Ca-ion batteries: a new energy storage system. *Chem. Mater.* **2015**, *27* (24), 8442–8447.
- (11) Cabello, M.; Nacimiento, F.; González, J. R.; Ortiz, G.; Alcántara, R.; Lavela, P.; Pérez-Vicente, C.; Tirado, J. L. Advancing towards a veritable calcium-ion battery: CaCo_2O_4 positive electrode material. *Electrochim. Commun.* **2016**, *67*, 59–64.
- (12) Park, H.; Cui, Y.; Kim, S.; Vaughey, J.; Zapol, P. Ca cobaltites as potential cathode materials for rechargeable Ca-ion batteries: theory and experiment. *J. Phys. Chem. C* **2020**, *124* (11), 5902–5909.
- (13) Tchitchevova, D. S.; Ponrouch, A.; Verrelli, R.; Broux, T.; Frontera, C.; Sorrentino, A.; Bardé, F.; Biskup, N.; Arroyo-de Domplab, M. E.; Palacin, M. R. Electrochemical intercalation of calcium and magnesium in TiS_2 : fundamental studies related to multivalent battery applications. *Chem. Mater.* **2018**, *30* (3), 847–856.
- (14) Kim, S.; Yin, L.; Bak, S.-M.; Fister, T. T.; Park, H.; Parajuli, P.; Gim, J.; Yang, Z.; Klie, R. F.; Zapol, P.; et al. Investigation of Ca insertion into $\alpha\text{-MoO}_3$ nanoparticles for high capacity Ca-ion cathodes. *Nano Lett.* **2022**, *22* (6), 2228–2235.
- (15) Park, H.; Zapol, P. Thermodynamic and kinetic properties of layered-Ca Co_2O_4 for the Ca-ion batteries: a systematic first-principles study. *J. Mater. Chem. A* **2020**, *8* (41), 21700–21710.
- (16) Dixit, M.; Kosa, M.; Lavi, O. S.; Markovsky, B.; Aurbach, D.; Major, D. T. Thermodynamic and kinetic studies of $\text{LiNi}_0.5\text{Co}_0.2\text{Mn}_0.3\text{O}_2$ as a positive electrode material for Li-ion batteries using first principles. *Phys. Chem. Chem. Phys.* **2016**, *18* (9), 6799–6812.
- (17) Risthaus, T.; Chen, L.; Wang, J.; Li, J.; Zhou, D.; Zhang, L.; Ning, D.; Cao, X.; Zhang, X.; Schumacher, G.; et al. P3 $\text{Na}_0.9\text{Ni}_0.5\text{Mn}_0.5\text{O}_2$ cathode material for sodium ion batteries. *Chem. Mater.* **2019**, *31* (15), 5376–5383.
- (18) Park, H.; Bartel, C. J.; Ceder, G.; Zapol, P. Layered Transition Metal Oxides as Ca Intercalation Cathodes: A Systematic First-Principles Evaluation. *Adv. Energy Mater.* **2021**, *11* (48), No. 2101698.
- (19) Juran, T. R.; Smeu, M. TiSe₂ cathode for beyond Li-ion batteries. *J. Power Sources* **2019**, *436*, No. 226813.
- (20) Mao, M.; Ji, X.; Hou, S.; Gao, T.; Wang, F.; Chen, L.; Fan, X.; Chen, J.; Ma, J.; Wang, C. Tuning anionic chemistry to improve kinetics of Mg intercalation. *Chem. Mater.* **2019**, *31* (9), 3183–3191.
- (21) Mo, Y.; Ong, S. P.; Ceder, G. Insights into diffusion mechanisms in P2 layered oxide materials by first-principles calculations. *Chem. Mater.* **2014**, *26* (18), 5208–5214.
- (22) Guo, S.; Sun, Y.; Yi, J.; Zhu, K.; Liu, P.; Zhu, Y.; Zhu, G.-z.; Chen, M.; Ishida, M.; Zhou, H. Understanding sodium-ion diffusion in layered P2 and P3 oxides via experiments and first-principles calculations: a bridge between crystal structure and electrochemical performance. *NPG Asia Mater.* **2016**, *8* (4), e266.
- (23) Rong, Z.; Malik, R.; Canepa, P.; Sai Gautam, G.; Liu, M.; Jain, A.; Persson, K.; Ceder, G. Materials design rules for multivalent ion mobility in intercalation structures. *Chem. Mater.* **2015**, *27* (17), 6016–6021.
- (24) Ramsdell, L. S. Studies on silicon carbide. *Am. Mineral.* **1947**, *32* (1–2), 64–82.
- (25) Huisman, R.; De Jonge, R.; Haas, C.; Jellinek, F. Trigonal-prismatic coordination in solid compounds of transition metals. *J. Solid State Chem.* **1971**, *3* (1), 56–66.
- (26) Kertesz, M.; Hoffmann, R. Octahedral vs. trigonal-prismatic coordination and clustering in transition-metal dichalcogenides. *J. Am. Chem. Soc.* **1984**, *106* (12), 3453–3460.
- (27) Stephenson, T.; Li, Z.; Olsen, B.; Mitlin, D. Lithium ion battery applications of molybdenum disulfide (MoS_2) nanocomposites. *Energy Environ. Sci.* **2014**, *7* (1), 209–231.
- (28) Savjani, N.; Lewis, E. A.; Bissett, M. A.; Brent, J. R.; Dryfe, R. A. W.; Haigh, S. J.; O'Brien, P. Synthesis of Lateral Size-Controlled Monolayer 1H- MoS_2 @Oleyamine as Supercapacitor Electrodes. *Chem. Mater.* **2016**, *28* (2), 657–664.
- (29) Liu, S.; Zeng, Y.; Zhang, M.; Xie, S.; Tong, Y.; Cheng, F.; Lu, X. Binder-free WS₂ nanosheets with enhanced crystallinity as a stable negative electrode for flexible asymmetric supercapacitors. *J. Mater. Chem. A* **2017**, *5* (40), 21460–21466.
- (30) Park, J.; Kim, J.-S.; Park, J.-W.; Nam, T.-H.; Kim, K.-W.; Ahn, J.-H.; Wang, G.; Ahn, H.-J. Discharge mechanism of MoS_2 for sodium ion battery: Electrochemical measurements and characterization. *Electrochim. Acta* **2013**, *92*, 427–432.
- (31) Ren, X.; Zhao, Q.; McCulloch, W. D.; Wu, Y. MoS_2 as a long-life host material for potassium ion intercalation. *Nano Res.* **2017**, *10*, 1313–1321.
- (32) Liao, Y.; Park, K.-S.; Singh, P.; Li, W.; Goodenough, J. B. Reinvestigation of the electrochemical lithium intercalation in 2H-and 3R- NbS_2 . *J. Power Sources* **2014**, *245*, 27–32.
- (33) Liao, Y.; Park, K.-S.; Xiao, P.; Henkelman, G.; Li, W.; Goodenough, J. B. Sodium Intercalation Behavior of Layered Na_xNbS_2 ($0 \leq x \leq 1$). *Chem. Mater.* **2013**, *25* (9), 1699–1705.
- (34) Blanc, L. E.; Choi, Y.; Shyamsunder, A.; Key, B.; Lapidus, S. H.; Li, C.; Yin, L.; Li, X.; Gwalani, B.; Xiao, Y.; et al. Phase stability and kinetics of topotactic dual Ca^{2+} – Na^+ ion electrochemistry in NaSICON $\text{NaV}_2(\text{PO}_4)_3$. *Chem. Mater.* **2023**, *35* (2), 468–481.
- (35) Hohenberg, P.; Kohn, W. Inhomogeneous electron gas. *Phys. Rev.* **1964**, *136* (3B), No. B864.
- (36) Kresse, G.; Furthmüller, J. Efficient iterative schemes for ab initio total-energy calculations using a plane-wave basis set. *Phys. Rev. B* **1996**, *54* (16), No. 11169.
- (37) Perdew, J. P.; Burke, K.; Ernzerhof, M. Generalized gradient approximation made simple. *Phys. Rev. Lett.* **1996**, *77* (18), No. 3865.
- (38) Kresse, G.; Joubert, D. From ultrasoft pseudopotentials to the projector augmented-wave method. *Phys. Rev. B* **1999**, *59* (3), No. 1758.
- (39) Yang, J.; Zhang, Y.; Ge, Y.; Tang, S.; Li, J.; Zhang, H.; Shi, X.; Wang, Z.; Tian, X. Interlayer engineering of layered materials for efficient ion separation and storage. *Adv. Mater.* **2024**, *36* (18), No. 2311141.
- (40) Jain, A.; Ong, S. P.; Hautier, G.; Chen, W.; Richards, W. D.; Dacek, S.; Cholia, S.; Gunter, D.; Skinner, D.; Ceder, G.; Persson, K. A. Commentary: The Materials Project: A materials genome approach to accelerating materials innovation. *APL Mater.* **2013**, *1* (1), No. 011002.
- (41) Levita, G.; Molinari, E.; Polcar, T.; Righi, M. C. First-principles comparative study on the interlayer adhesion and shear strength of transition-metal dichalcogenides and graphene. *Phys. Rev. B* **2015**, *92* (8), No. 085434.
- (42) Levita, G.; Cavaleiro, A.; Molinari, E.; Polcar, T.; Righi, M. C. Sliding properties of MoS_2 layers: load and interlayer orientation effects. *J. Phys. Chem. C* **2014**, *118* (25), 13809–13816.
- (43) Henkelman, G.; Jónsson, H. Improved tangent estimate in the nudged elastic band method for finding minimum energy paths and saddle points. *J. Chem. Phys.* **2000**, *113* (22), 9978–9985.
- (44) Henkelman, G.; Überuaga, B. P.; Jónsson, H. A climbing image nudged elastic band method for finding saddle points and minimum energy paths. *J. Chem. Phys.* **2000**, *113* (22), 9901–9904.
- (45) Sun, W.; Dacek, S. T.; Ong, S. P.; Hautier, G.; Jain, A.; Richards, W. D.; Gamst, A. C.; Persson, K. A.; Ceder, G. The thermodynamic scale of inorganic crystalline metastability. *Sci. Adv.* **2016**, *2* (11), No. e1600225.
- (46) Li, B.; Zhou, B.; Qu, Z.; Song, Q.; Jiang, Z. Theoretical study on Fe₂C MXene as electrode material for secondary battery. *Chem. Phys.* **2021**, *548*, No. 111223.

(47) Wang, S.; Fu, J.; Liu, Y.; Saravanan, R. S.; Luo, J.; Deng, S.; Sham, T.-K.; Sun, X.; Mo, Y. Design principles for sodium superionic conductors. *Nat. Commun.* **2023**, *14* (1), No. 7615.

(48) Canepa, P.; Bo, S.-H.; Sai Gautam, G.; Key, B.; Richards, W. D.; Shi, T.; Tian, Y.; Wang, Y.; Li, J.; Ceder, G. High magnesium mobility in ternary spinel chalcogenides. *Nat. Commun.* **2017**, *8* (1), No. 1759.

(49) Zhang, L.; Yang, K.; Mi, J.; Lu, L.; Zhao, L.; Wang, L.; Li, Y.; Zeng, H. Na₃PSe₄: A Novel Chalcogenide Solid Electrolyte with High Ionic Conductivity. *Adv. Energy Mater.* **2015**, *5* (24), No. 1501294.